UCRL-17475

University of California

Ernest O. Lawrence Radiation Laboratory

REGGE TRAJECTORIES FOR TWO YUKAWA POTENTIALS

TWO-WEEK LOAN COPY

This is a Library Circulating Copy which may be borrowed for two weeks. For a personal retention copy, call Tech. Info. Division, Ext. 5545

DISCLAIMER

This document was prepared as an account of work sponsored by the United States Government. While this document is believed to contain correct information, neither the United States Government nor any agency thereof, nor the Regents of the University of California, nor any of their employees, makes any warranty, express or implied, or assumes any legal responsibility for the accuracy, completeness, or usefulness of any information, apparatus, product, or process disclosed, or represents that its use would not infringe privately owned rights. Reference herein to any specific commercial product, process, or service by its trade name, trademark, manufacturer, or otherwise, does not necessarily constitute or imply its endorsement, recommendation, or favoring by the United States Government or any agency thereof, or the Regents of the University of California. The views and opinions of authors expressed herein do not necessarily state or reflect those of the United States Government or any agency thereof or the Regents of the University of California.

Submitted to The Physical Review

UCRL-17475
Preprint

UNIVERSITY OF CALIFORNIA

Lawrence Radiation Laboratory
Berkeley, California

AEC Contract No. W-7405-eng-48

REGGE TRAJECTORIES FOR TWO YUKAWA POTENTIALS

N. F. Bali, Shu-Yuan Chu, Richard W. Haymaker,
and Chung-I Tan

April 3, 1967

UCRL-17475

REGGE TRAJECTORIES FOR TWO YUKAWA POTENTIALS*

N. F. Bali,† Shu-Yuan Chu, Richard W. Haymaker
and Chung-I Tan

Lawrence Radiation Laboratory
University of California
Berkeley, California

April 3, 1967

ABSTRACT

The leading Regge trajectories generated by two Yukawa potentials of different ranges are studied by both analytical and numerical methods. We find that several new features appear which are not present in the single Yukawa case. We investigate in detail the behavior of the trajectories as we change gradually from the single to the two Yukawa potential case, paying close attention to the appearance of branch cuts other than the usual right hand cut in the leading trajectories. We notice that these cuts, if present in relativistic theory, can play important roles in explaining effects such as the polarization in the $\pi^- p$ charge exchange reaction.

I. INTRODUCTION

Regge trajectories for a single attractive or repulsive Yukawa potential have been extensively investigated both by analytical and by numerical methods.[1-4] Studies of potential theory have served as one of the main sources of intuition concerning Regge trajectories in strong interaction physics. However, it is extremely unlikely that single attractive or repulsive Yukawa potentials are a good approximation to nuclear forces. Such potentials are unable to model attractive forces with repulsive cores or long range repulsions; these forces are believed to be important components of the strong interaction.[5]

This paper describes a study of the behavior of Regge trajectories that arise from a superposition of two Yukawa potentials of different ranges. In particular, we shall be interested in the behavior of the trajectories for negative energies, as this is the region which, in the relativistic case, controls the asymptotic behavior of the crossed channel, and thus has direct experimental consequences. Our technique will be to use analytical methods to investigate the features in the weak coupling limit, and then use numerical solutions of the Schrödinger equation to ascertain which features remain true in the more realistic strong coupling case. We will be able to determine the positions of the singularities of the trajectory functions, which

are quite different from the single Yukawa case. This, in turn, will affect phenomenological formulae used in high energy data fitting.

In Section II we review, for completeness, the equations for the trajectories in the weak coupling limit. In Section III, we exhibit the main results of the weak coupling limit, which are justified in Section IV. Section V includes numerical calculations of the strong coupling case.

II. MATHEMATICAL PRELIMINARIES

For scattering of a spinless particle of mass m by a central potential $V(r)$, the ℓth partial wave S-matrix element is uniquely determined by the Jost function $f_+(\ell,k)$, through the equation[6]

$$S(\ell,k) = \frac{f_+(\ell,k)}{f_+(\ell,k\, e^{-i\pi})} \equiv \frac{f_+(\ell,k)}{f_-(\ell,k)} . \tag{II.1}$$

For our purposes, we assume the potential to be sufficiently analytic at the origin so that the Jost function $f_+(\ell,k)$ is an analytic function of ℓ, with fixed poles possibly for $\mathrm{Re}\,\ell < -\frac{1}{2}$. The Jost function can be defined in terms of the radial wave function[6] $\phi(\ell;k,r)$:

$$f_\pm(\ell,k) = 1 \mp \frac{\pi}{2}\, i \frac{(\frac{1}{2}k)^{\ell+\frac{1}{2}}}{\Gamma(\ell + 3/2)} \int_0^\infty \left(2mV(r)\right) r^{\frac{1}{2}}\, H^{\binom{2}{1}}_{\ell+\frac{1}{2}}(kr)\, \phi(\ell;k,r)\, dr , \tag{II.2}$$

where the Hankel function is related to the Bessel function $J_{\ell+\frac{1}{2}}(kr)$ by:

$$H^{\binom{2}{1}}_{\ell+\frac{1}{2}}(kr) = (i \tan \ell\pi \pm 1)\, J_{\ell+\frac{1}{2}}(kr) + \frac{i}{\cos \ell\pi}\, J_{-\ell-\frac{1}{2}}(kr). \tag{II.3}$$

The wave function $\phi(\ell;k,r)$ is normalized to satisfy the boundary condition:

$$\lim_{r \to 0} \frac{\phi(\ell;k,r)}{r^{\ell+1}} = 1. \tag{II.4}$$

This normalization together with the fact that $J_\lambda(z) = J_{-\lambda}(z)$ at integral values of λ ensures that $f_\pm(\ell,k)$ will not have fixed poles at negative half-integral values[6] of ℓ.

The singularities of $f_\pm(\ell,k)$ in the ℓ plane come from the divergence of the integral in Eq. (II.2) at its lower limit.[7] For $\mathrm{Re}\,\ell > -\frac{1}{2}$, this will not happen. As we go into the left-half ℓ plane, $f_\pm(\ell,k)$ can have simple poles. For potentials that behave like $r^{2n-1} + f(r^2)$ near origin, n an integer greater or equal to 0, we see that $f_\pm(\ell,k)$ has simple poles[8] at $\ell = -n-1, -n-2, \cdots$. The residues of these poles, of course, depend on the potential. In particular, some of them may be equal to zero for special values of k.

The analytic properties of $f_-(\ell,k)$ in the k plane are well known. The Jost function $f_-(\ell,k)$ has a left-hand cut along the negative imaginary axis in the k plane. It also has a root type branch point of order $2\ell + 1$ at $k = 0$.

From Eq. (II.1), one sees that the poles of $S(\ell,k)$ are given by the zeros of $f_-(\ell,k)$. Consequently, the Regge trajectory

function $\alpha(k^2)$ is a multi-valued function of k^2, satisfying the following equation[9]

$$f_-\left(\ell = \alpha(k^2), k\right) = 0 \quad \text{for all} \quad k. \tag{II.5}$$

By the implicit function theorem, $\alpha(k^2)$ has all the singularities of $f_-(\ell,k)$ and also has additional root-type branch points, whenever

$$f_-\left(\alpha(k^2), k\right) = \left(\frac{df_-(\ell,k)}{d\ell}\right)_{\ell=\alpha(k^2)} = \cdots = \left(\frac{d^{(m)}f_-(\ell,k)}{d\ell^{(m)}}\right)_{\ell=\alpha(k^2)} = 0 \ . \tag{II.6}$$

This corresponds to the coincidence of zeros of $f_-(\ell,k)$. It is this possibility of multiple zeros that allows $\alpha(k^2)$ to have the special singularity structure that will be described below.

For our analysis, we shall evaluate the Jost function $f_-(\ell,k)$ for a superposition of Yukawa potentials in the weak coupling limit.[10] Let $V(r) = \sum_s g_s \frac{e^{-\mu_s r}}{r}$ and approximate $\phi(\ell;k,r)$ by a free wave function, with the normalization of Eq. (II.4). We immediately find, from Eq. (II.2), that

$$f_-(\ell,k) = 1 - \sum_s \frac{mg_s e^{-i\pi\ell}}{\cos \pi\ell} \left(\frac{1}{ik}\right) Q_\ell\left(1 + \frac{\mu_s^2}{2k^2}\right) + \sum_s \frac{mg_s}{k}$$

$$\times \frac{1}{\cos \pi\ell} \quad R_\ell\left(1 + \frac{\mu_s^2}{2k^2}\right) \tag{II.7}$$

where[11]

$$Q_\ell\left(1 + \frac{\mu^2}{2k^2}\right) = (\pi k)\int_0^\infty e^{-\mu x} J^2_{\ell+\frac{1}{2}}(kx)\, dx \quad , \tag{II.8}$$

and

$$R_\ell\left(1 + \frac{\mu^2}{2k^2}\right) = (\pi k)\int_0^\infty e^{-\mu x} J_{\ell+\frac{1}{2}}(kx)\, J_{-\ell-\frac{1}{2}}(kx)\, dx \ . \tag{II.9}$$

Since R_ℓ is an entire function of ℓ and $Q_\ell = R_\ell$ at half integral value of ℓ, we see that the only singularities of $f_-(\ell,k)$ in ℓ come from poles of Q_ℓ at $\ell = -1, -2, \cdots$. The residues at $\ell = -N$ are given by $-\sum_s \frac{mg_s}{ik} P_{N-1}\left(1 + \frac{\mu_s^2}{2k^2}\right)$.

III. PROPERTIES OF $\alpha(k^2)$ IN THE WEAK COUPLING LIMIT: DESCRIPTION

In this section we shall describe, without proof, the main features of $\alpha(k^2)$ in the weak coupling limit. Our discussion will be, for the most part, qualitative, yet all of the features described have been observed in numerical calculations for weak potentials.

Our results can be summarized most easily by considering what happens to a given set of trajectories when the potential strengths are varied. As a matter of procedure, we shall start with a pure short range component of the potential, then introduce a long range component gradually until the strengths are equal, and finally reduce the strength of the short range component to zero. We shall study the effect of these variations in the potential on the trajectory configurations. The initial and final configurations of this sequence have been described in great detail,[2] and some information on the intermediate stages exists.[12,13] We shall attempt to make this more systematic, and we expect to gain some understanding of the singularity structure of $\alpha(k^2)$.

The potential under consideration is the following:

$$V(r) = V_1(r) + V_2(r) , \qquad \text{(III.1)}$$

where $V_i(r) = g_i \frac{e^{-\mu_i r}}{r}$ for $i = 1, 2$. We shall always take $\mu_1 < \mu_2$, i.e., V_1 will be the long range component of the potential. There are then four possible cases to consider, with the one used depending on the signs of g_1 and g_2. We use the convention that $g_i < 0$ corresponds to an attractive potential.

(A) $\underline{g_1 < 0, \quad g_2 > 0}$

This is the case of long range attractive and short range repulsion, corresponding to an attractive force with a repulsive core. The complete sequence is shown in Fig. 1, where we also indicate the cuts structure in the k^2 plane of one of the trajectories.

The initial configuration (Fig. 1a) is that of a pure repulsive potential.[2] One trajectory goes to each negative integer for $k^2 \to -\infty$. As k^2 increases from $-\infty$, the poles at the even negative integers move to the right and collide with those at the odd negative integers which move to the left. After the collision, the poles "bounce" into the complex ℓ plane as complex conjugate pairs,[14] and reach $\ell = -\frac{1}{2}$ from above and below as $k^2 \to 0$. Above threshold, half the poles return to the negative integers and half of them go off to infinity in the second quadrant.

At the other extreme of the sequence (Fig. 2i), the purely attractive case, the pattern is quite similar except that even poles now move to the left. The pole which starts at $\ell = -1$ does not collide with any other pole, and reaches a point on the

real axis beyond $\ell = -\frac{1}{2}$ at $k^2 = 0$. Above threshold, this pole returns to $\ell = -1$ through an excursion in the upper half ℓ plane. This is the leading trajectory. It is the only one that satisfies a dispersion relation with a cut from threshold to infinity.[15] All the other poles behave in a way similar to the repulsive case.

As the attractive long-range potential is turned on, so that $\left|\frac{g_1}{\mu_1}\right| > \left|\frac{g_2}{\mu_2}\right|$, the trajectories which start at $\ell = -1$ and -2 no longer reach $\ell = -\frac{1}{2}$ but collide on the real axis to the left of $\ell = -\frac{1}{2}$ as shown in Fig. 1b. After that, the one from -2 goes on to the right and reaches

$$\ell_0 = -\tfrac{1}{2} + \left(-\frac{g_1}{\mu_1} - \frac{g_2}{\mu_2}\right) > -\tfrac{1}{2}\,, \tag{III.2}$$

at threshold, while the one from -1 turns back and reaches

$$\ell_0 = -1 + \tfrac{1}{2}\,\frac{\ln\left(-\frac{g_1}{g_2}\right)}{\ln\left(\frac{\mu_1}{\mu_2}\right)}\,, \tag{III.3}$$

at threshold. These threshold values are marked with a dot (III.2) and a cross (III.3) in Fig. 1. The leading trajectory, which in this case is the one from $\ell = -2$, now has a finite cut for $k^2 < 0$, which can extend arbitrarily close to threshold, due to the collisions with the pole from $\ell = -1$.

Increasing the attraction further takes us to $|g_1| = |g_2|$, at which point the trajectory starting at $\ell = -1$ completely disappears, since the potential no longer has a $\frac{1}{r}$ singularity at the origin. The disappearance is achieved by the collapse of the "bubble" which surrounded $\ell = -1$ as shown in Figs. 1b and 1c. Equivalently the two branch points of the finite cut for $k^2 < 0$ of the trajectory from $\ell = -2$ coincide. At this point, if we start reducing the repulsion, the roles of the trajectories from $\ell = -1$ and -2 become interchanged. This "interchange" can be best understood by noticing that in the k^2 plane, the trajectory from $\ell = -2$ has two new complex branch points (Fig. 1d), so a path along the negative k^2 axis necessarily goes above one and below the other.

Upon further reduction of the repulsion, the threshold value of the trajectory from $\ell = -2$ decreases until it is below -2, while two complex conjugate branch points, corresponding to its collision with trajectories from -3, approach the negative k^2 axis (Fig. 1e). In Fig. 1f, the two branch points have collided and diverged along the real axis. The trajectory from $\ell = -2$ now collides with the one from -4, since the latter interchanged its role with the one from -3 after the two branch points collided. If we continue decreasing the repulsion the story repeats itself: the bubble surrounding $\ell = -3$ collapses and the poles from $\ell = -3$ and -4 switch roles. In the end as the repulsion goes to zero, this

mechanism has propagated itself to $\ell = -\infty$ and we arrive at the configuration of pure attraction[2] as shown in Fig. 1i.

There is a further complication to the switch over described above. When $\left|\frac{g_1}{\mu_1}\right|$ exceeds $\left|\frac{g_2}{\mu_2}\right|$ an infinite number of poles go to complex values of ℓ at $k^2 = 0$. These zeros of $f_-(\ell,k)$ accompany the one on the real axis mentioned above and marked by "x" in Fig. 1. Their real part at threshold is the same and is given by Eq. (III.3). They are equally spaced along the imaginary axis. Their imaginary parts are:

$$\mathrm{Im}\,\alpha(0) = n\left(\frac{\pi}{\ln\frac{\mu_2}{\mu_1}}\right) \quad \text{for } n = 0;\ \pm 1;\ \pm 2;\cdots\cdots \qquad \text{(III.4)}$$

As k^2 approaches zero, each trajectory spirals an infinite number of times around its threshold value[13] as shown in Fig. 2. There are still an infinite number of trajectories going to $\ell = -\frac{1}{2}$ at $k^2 = 0$. As the vertical line of threshold values moves to the left, as shown by the advance of the mark "x" in Fig. 1, the spiraling trajectories collide with neighboring ones, and switch roles, much in the same way as the trajectories of real threshold values do. As the repulsion is reduced, the complex-threshold trajectories connect to larger and larger negative integers. Finally, as the potential is made purely attractive, the vertical line of threshold values, and the connecting trajectories are

all swept to the left to infinity, and all trajectories except the leading one go to $\ell = -\frac{1}{2}$ at threshold.

(B) $g_1 > 0$, $g_2 < 0$

In this case we are dealing with a short range attraction and a long range repulsion. The sequence now runs from pure attraction to pure repulsion.

The detailed manner in which the switch over takes place is analogous to case A, and thus we shall discuss it only briefly.

Unlike case (A), however, there are no branch points on the negative real k^2 axis for the trajectory which passes $\ell = -\frac{1}{2}$ for $k^2 < 0$ (leading-like trajectory). It also does not have complex branch points until $|g_1| > |g_2|$, for it could not "lie down" and disappear when $|g_1| = |g_2|$. Once $|g_1| > |g_2|$, complex branch points will appear in the ℓ plane which are necessary to carry out the switch over of trajectories. The entire sequence similar to that of Fig. 1 is shown in Fig. 3.

Complex threshold values will again accompany the real threshold value marked by "x" in Fig. 3. The positions of the complex threshold are still given by formulas III.3 and III.4.

(C) $g_1 < 0$, $g_2 < 0$ or $g_1 > 0$, $g_2 > 0$

These cases include the combination of attractive or repulsive potentials of different ranges, and are quite similar to the single Yukawa potential. We want to note only that complex threshold values

for some trajectories are again possible once $\left|\frac{g_1}{\mu_1}\right| > \left|\frac{g_2}{\mu_2}\right|$.

The line of the complex threshold values moves left as $|g_1|$ increases. Its position is given by

$$\mathrm{Re}\ \ell_0 = -1 - \frac{1}{2}\,\frac{\ln\left|\frac{g_1}{g_2}\right|}{\ln\left|\frac{\mu_1}{\mu_2}\right|} \quad . \tag{III.5}$$

The imaginary parts of the complex thresholds are

$$\mathrm{Im}\ \ell_0 = \left(n + \tfrac{1}{2}\right)\frac{\pi}{\ln\left(\frac{\mu_1}{\mu_2}\right)} \quad \text{for} \quad n = 0;\ \pm 1;\ \pm 2, \cdots \ . \tag{III.6}$$

IV. PROPERTIES OF $\alpha(k^2)$ IN THE WEAK COUPLING LIMIT: JUSTIFICATION

As noted in Sec. II, the Regge trajectory function $\alpha(k^2)$ is given by the solution of the following equation:

$$f_-\left(\ell = \alpha(k), k\right) = 0 \ . \tag{IV.1}$$

Our discussion will be divided into two parts. In part A, we study the properties of $\alpha(k^2)$ for finite k^2. In part B, we discuss the situation when k^2 approaches threshold. From these we can get a qualitative picture of $\alpha(k^2)$ as described in the previous section.

(A) Collision of Poles

For a finite region in the ℓ and k^2 planes not including $k^2 = 0$, we can subtract out the fixed poles of $f_-(\ell,k)$ and expand what remains in a multiple power series in $(\ell-\ell_0)$ and $(k^2-k_0{}^2)$.

$$f_-(\ell,k) + \sum_{n,s} \frac{g_s{}^m}{ik} \frac{\Pr\left(1 + \frac{\mu_s{}^2}{2k^2}\right)}{\ell + n + 1} = \sum_{m,n=0}^{\infty} a_{mn}(\ell-\ell_0)^m \left(k^2-k_0{}^2\right)^n, \tag{IV.2}$$

where a_{00} is of order 1, and all the other a's are of order g. We subtract out the poles at $\ell = -1$ and -2 to study the behavior of the Jost function in this region. When only the first term of Eq. (IV.2) is kept, Eq. (IV.1) reduces to a quadratic equation in ℓ. In the case of two Yukawa potentials we have

$$\ell^2 + \left(\frac{2m\, v_0}{\kappa} - \frac{m\, v_2}{\kappa^3} + 3\right)\ell + \left(\frac{3m\, v_0}{\kappa} - \frac{m\, v_2}{\kappa^3} + 2\right) = 0 \,, \qquad \text{(IV.3)}$$

where $\kappa = -ik$, $v_0 = g_1 + g_2$, and $v_2 = \frac{1}{2}(g_1\, \mu_1^{\,2} + g_2\, \mu_2^{\,2})$. The solutions of this equation give us two Regge trajectories. They are:

$$\alpha(k^2) = -\frac{b}{2} \pm \frac{1}{2}\,(b^2 - 4c)^{\frac{1}{2}} \qquad \text{(IV.4)}$$

where

$$b = \frac{2m\, v_0}{\kappa^2} - \frac{m\, v_2}{\kappa^3} + 3$$

$$c = \frac{3m\, v_0}{\kappa} - \frac{m\, v_2}{\kappa^3} + 2 \,. \qquad \text{(IV.5)}$$

Equation (IV.4) shows explicitly that two Regge trajectories are different branches of the same analytic function. The branch points are given by the zeros of the discriminant $D(\kappa) = b^2 - 4c$, or

$$D(\kappa) = \left(1 - \frac{m\, v_2}{\kappa^3}\right)^2 + \frac{4v_0\, m^2}{\kappa^2}\left(v_0 - \frac{v_2}{\kappa^2}\right) = 0 \,. \qquad \text{(IV.6)}$$

Let us look at the behavior of $\alpha(k^2)$ as we vary k^2 from $-\infty$, to the threshold along the real axis. For large κ, $D(\kappa) \approx 1 > 0$, so $\alpha(k^2)$ is real. When $\kappa \to \infty$, $\alpha(k^2)$ approaches $\ell = -1$ and -2. If $D(\kappa)$ becomes negative as we decrease κ, these two trajectories first come together at the point $D(\kappa) = 0$, and then bounce off into a pair of complex conjugate poles in the ℓ plane. The singularity structure of $\alpha(k^2)$ can be found by studying the location of zeros of $D(\kappa)$. Before we proceed further, a word of

caution is in order. Since Eq. (IV.3) is an approximation, one has to examine its validity when going to small values of κ. It will be incorrect when $\frac{\kappa^2}{\mu^2} \ll 1$. But the information contained in the solution of Eq. (IV.3) is rich enough for our discussion. The behavior when $\frac{\kappa^2}{\mu^2} \approx 0$ will be discussed in part B of this section.

Let us see how the positions of the branch points depend on the relative value of g_1 and g_2. Take, for example, case A of Sec. II. We have a combination of long range attraction and short range repulsion, i.e., $g_1 < 0$, $g_2 > 0$.

(i) $\underline{-g_1 > g_2 > 0,\ |g_1 \mu_1^2| > |g_2 \mu_2^2|,\ \text{i.e.},\ v_0 < 0,\ v_2 > 0}$

Here we have a long range attraction with small repulsive core. Since $D(\kappa)$ is always positive for $0 < \kappa < \infty$, we do not have real branch points; instead, there are two complex conjugate branch points (Fig. 1d, but notice that in this approximation the collision with the trajectory from -3 is not described.).

(ii) $\underline{-g_1 = g_2 > 0,\ \text{i.e.},\ v_0 = 0,\ v_2 > 0}$

As we decrease the attraction, these two branch points move onto the real axis. The coincidence of two branch points, at $\kappa^3 = m\, v_2$, has the effect of "decoupling" these two trajectories (Fig. 1c). In fact, Eq. (IV.3) factors into the form $(\ell + 1)\left(\ell + 2 - \frac{m\, v_2}{\kappa^3}\right) = 0$, so that one pole remains at $\ell = -1$, and the one from $\ell = -2$ actually does not have a branch point. We see that $D(\kappa)$ has a double zero, but remains positive

along the negative k^2 axis.

(iii) $\underline{0 < -g_1 < g_2, \quad |g_1/\mu_1| > |g_2/\mu_2|}$

As we further decrease the attraction, $D(\kappa)$ will have a pair of zeros on the real axis (Fig. 1b); thus $\alpha(k^2)$ has two real branch points.

(iv) $\underline{g_1 = 0, \; g_2 > 0}$

When we remove the attraction completely, one of the two branch points will have moved to threshold (Fig. 1a). There will be one branch point at $\kappa \approx (2g_2^{\;2}\,\mu_2^{\;2})^{1/3}$ where the two trajectories from $\ell = -1$ and -2 collide.

Similarly, we can study other combinations of Yukawa potentials, or the behavior of trajectories from other negative integral values of ℓ, using the above technique.

(B) Threshold Behavior

To complete the picture, we have to examine the Jost function $f_-(\ell,k)$ near $k^2 = 0$. We have the following asymptotic behavior[11] for Q_ℓ and R_ℓ as $k \to 0$

$$Q_\ell\left(1 + \frac{\mu^2}{2k^2}\right) \sim \sqrt{\pi}\,\frac{\Gamma(\ell + 1)}{\Gamma(\ell + 3/2)}\left(\frac{k^2}{\mu^2}\right)^{\ell+1} \tag{IV.7}$$

$$R_\ell\left(1 + \frac{\mu^2}{2k^2}\right) \sim \frac{\sin[\pi(2\ell + 1)]}{(2\ell + 1)}\,\frac{k}{\mu} \tag{IV.8}$$

Substituting (IV.7) and (IV.8) into Eq. (II.7), we have

$$f_-(\ell,k) \approx C_1(\ell)\left\{1 + \frac{C_2(\ell)}{C_1(\ell)} \quad \kappa^{2\ell+1}\right\} \tag{IV.9}$$

where

$$C_1(\ell) \equiv 1 + \frac{m}{\cos \pi\ell} \frac{\sin[(2\ell+1)\pi]}{(2\ell+1)} \left(\frac{g_1}{\mu_1} + \frac{g_2}{\mu_2}\right) \tag{IV.10}$$

$$C_2(\ell) \equiv \frac{m}{\cos \pi\ell} \sqrt{\pi} \frac{\Gamma(\ell+1)}{\Gamma(\ell+3/2)} \left(g_1 \mu_1^{-2\ell-2} + g_2 \mu_2^{-2\ell-2}\right) \tag{IV.11}$$

Equation (IV.1) then reduces to[16]

$$1 + \frac{C_2(\ell)}{C_1(\ell)} \quad \kappa^{2\ell+1} = 0 \ . \tag{IV.1'}$$

The solutions of Eq. (IV.1') can be classified according to whether Re $[\alpha(k^2 = 0)]$ is greater than, equal to or smaller than $-\frac{1}{2}$.

(i) <u>Real solution to the right of $\ell = -\frac{1}{2}$</u>

Since $\kappa^{2\ell+1} \to 0$ as $\kappa \to 0$ for $\mathrm{Re}\,\ell > -\frac{1}{2}$, Eq. (IV.1') has solutions only at poles of $\left(C_2(\ell)/C_1(\ell)\right)$, which are given by the zeros of $C_1(\ell)$. In the weak coupling limit it will be near $\ell = -\frac{1}{2}$. Solving $C_1(\ell) = 0$, we obtain

$$\ell \approx -\tfrac{1}{2} - m\left(\frac{g_1}{\mu_1} + \frac{g_2}{\mu_2}\right) \ . \tag{IV.12}$$

Since we require $\ell > -\frac{1}{2}$, we see that there will be a pole moving to the right of $\ell = -\frac{1}{2}$ as $k^2 \to 0$, provided $\frac{g_1}{\mu_1} + \frac{g_2}{\mu_2} < 0$. (See Fig. 1b).

(ii) Real solutions at $\ell = -\frac{1}{2}$

This is the commonly known threshold behavior that has been discussed in many places.[4] We discuss here the features of two Yukawa potentials. Letting $\ell = -\frac{1}{2} + \Delta\ell$, the constant $C_1(\ell)$ and $C_2(\ell)$ have the following behavior near $\ell = -\frac{1}{2}$:

$$C_1(-\tfrac{1}{2} + \Delta\ell) \approx 1 + \frac{m}{\Delta\ell}\left(\frac{g_1}{\mu_1} + \frac{g_2}{\mu_2}\right)$$

$$C_2(-\tfrac{1}{2} + \Delta\ell) \approx \frac{m}{\Delta\ell}\left\{g_1\,\mu_1^{-1-2\Delta\ell} + g_2\,\mu_2^{-1-2\Delta\ell}\right\} . \qquad \text{(IV.13)}$$

(a) If $\frac{g_1}{\mu_1} + \frac{g_2}{\mu_2} \neq 0$, we have

$$\frac{C_1(-\frac{1}{2})}{C_2(-\frac{1}{2})} = 1 . \qquad \text{(IV.14)}$$

It then follows from Eq. (IV.1') that

$$\ell = -\tfrac{1}{2} + \frac{\pm 2\pi i p}{\ln\,(\kappa^2/\mu_1\mu_2)} \;;\; p = 1, 2, 3, \cdots \qquad \text{(IV.15)}$$

Thus all poles approach $\ell = -\frac{1}{2}$ in a complex direction in the ℓ plane.

(b) If $\frac{g_1}{\mu_1} + \frac{g_2}{\mu_2} = 0$, Eq. (IV.14) will no longer be true. We find

$$\ell = -\tfrac{1}{2} + \frac{\ln\left[C_1(-\frac{1}{2})/C_2(-\frac{1}{2})\right] \pm 2\pi i p}{\ln\,(\kappa^2/\mu_1\mu_2)} \quad p = 0, 1, 2, \cdots . \qquad \text{(IV.16)}$$

Now we have one trajectory approaching $\ell = -\frac{1}{2}$ along the real axis. This agrees with the solution given in (i).

(iii) <u>Solutions to the left of $\mathrm{Re}\,\ell = -\frac{1}{2}$ and complex thresholds</u>

Since $\kappa^{2\ell+1} \to \infty$ as $\kappa \to 0$ for $\mathrm{Re}\,\ell < -\frac{1}{2}$, solutions of Eq. (IV.1') must have threshold values at the zeros of $C_2(\ell)$. These are the points ℓ_0 such that

$$g_1\,\mu_1^{-2\ell_0-2} + g_2\,\mu_2^{-2\ell_0-2} = 0 . \qquad \text{(IV.17)}$$

We distinguish the following cases:

(a) $g_1 < 0,\ g_2 > 0$; or $g_1 > 0,\ g_2 < 0$ (See Sections IIIA, IIIB)

Equation (IV.17) gives us

$$\mathrm{Re}\,\ell_0 = -1 + \tfrac{1}{2}\,\frac{\ln\left(-\frac{g_1}{g_2}\right)}{\ln\left(\frac{\mu_1}{\mu_2}\right)}$$

$$\mathrm{Im}\,\ell_0 = \pm\,\frac{p\pi}{\ln\left(\frac{\mu_1}{\mu_2}\right)} \quad p = 0, 1, 2, \cdots . \qquad \text{(IV.18)}$$

Since these points are constrained by the fact that $\mathrm{Re}\,\ell_0 < -\frac{1}{2}$ and $\mu_1 < \mu_2$ by convention, we see that they exist only if either $|g_1| > |g_2|$, or $|g_1| < |g_2|$ and $|g_1/\mu_1| < |g_2/\mu_2|$. In either case there is a solution on the negative real ℓ axis.

(b) $g_1 > 0,\ g_2 > 0$; or $g_1 < 0,\ g_2 < 0$ (See Sec. III C)

In this case, we have no solution on the real ℓ axis. All solutions are complex with the same real part as given by Eq. (IV.18). The imaginary parts are given by

$$\mathrm{Im}\,\ell_0 = \pm \frac{\left(\frac{2p+1}{2}\right)\pi}{\ln\left(\frac{\mu_1}{\mu_2}\right)} \quad p = 0, 1, 2, \cdots . \tag{IV.19}$$

Near ℓ_0 the behavior of the trajectories as $\kappa \to 0$ is given by

$$\alpha(k^2) = \ell_0 + \text{const. } x(\kappa)^{-(2\ell_0 + 1)} . \tag{IV.20}$$

We see that $\alpha(k^2)$ executes infinitely many spirals[13] in approaching the point ℓ_0.

V. STRONG COUPLING CONFIGURATION

The analytic methods used in the preceding sections to study the weak coupling limit for two Yukawa potentials cannot be used when the coupling becomes strong. It is clear that the realistic potentials are in fact quite strong, so it is of interest to ascertain what features of the weak coupling limit remain valid in this case, and whether new features develop. To clarify this point, we have carried out extensive numerical investigation of the two-Yukawa-potential Schrödinger equation using a variational method.[17] These investigations allowed us to conclude that most of the features described in the preceding sections remain true. One important difference, however, is that if the attraction is sufficiently strong, several leading-like trajectories can be present. We shall describe the strong coupling case by giving a few examples of the typical trajectory configurations that have been studied.

(A) $g_1 < 0,\ g_2 > 0$

As in the weak coupling limit, the configuration of a short range repulsion with a long range attraction can give rise to leading trajectories which collide with neighboring ones and have real branch points for $k^2 < 0$. Such a case is exhibited in Figs. 4-6. Trajectory from $\ell = -2$ is now the leading one. It has branch points at $k^2 = -0.35$ and $k^2 = -0.02$, besides the

usual branch point at $k^2 = 0$. Another example of this phenomenon, but corresponding to a longer range attraction is shown in Fig. 7. Trajectory from $\ell = -2$ reaches much further into the right half ℓ plane. The trajectory from $\ell = -3$ is also a leading trajectory with extra branch points. As $k^2 \to +\infty$ the trajectories from $\ell = -1$ and -3 have switched roles, indicating that each trajectory has a complex branch point in the k^2 plane. A path in the k^2 plane which goes from $-\infty$ to $+\infty$ along the real axis will have circled this branch cut once. The trajectories from $\ell = -1$ and -3 are therefore not closed.

(B) $\underline{g_1 > 0,\ g_2 < 0}$

The configuration of a long range repulsion and a short range attraction is also very interesting, as we expect that the effect of inelastic channels can be modeled by a long range repulsion. An example of such trajectory is shown in Fig. 6. One outstanding feature of these trajectories is that even though the $k^2 = 0$ intercept is to the left of $\ell = 0$, they are still able to reach past $\ell = 0$, forming an S-wave resonance.[18] This can be easily understood by noticing that the long range repulsion and a short range attraction can form a well to contain resonances. In Fig. 8 we give an example of such an S-wave resonance in the leading trajectory, together with a leading-like trajectory from $\ell = -2$.

The effects of long range repulsion are also present for resonances of $\ell > 0$, since it enhances the barrier that contains them.

In particular, if we consider a resonance at $k^2 = k_R^2$ and we increase the repulsion and correspondingly the attraction, so that the resonance energy remains constant, we find that the width becomes narrower. We have defined the width as:

$$\Gamma \approx \frac{2\,\mathrm{Im}\alpha}{\left(\frac{d}{dk^2}\,[\mathrm{Re}\alpha]\right)_{k^2 = k_R^2}} \tag{V.1}$$

In Table I we give an actual example. As in the weak coupling case, we expect the leading trajectory to have no complex branch point as long as the strength of the repulsion is, in absolute value, less than the strength of the attraction.

(C) $\underline{g_1 < 0,\ g_2 < 0;\ \ g_1 > 0,\ g_2 > 0}$

The behavior of the trajectories when both potentials are of the same sign does not have any important new feature not present in the weak coupling case, except, of course, we may have several leading-like trajectories for attractive potentials.

VI. CONCLUSION

Not all the features described in the preceding sections will have direct consequences for high energy Regge-pole fitting since the quantitative relation between realistic trajectories and those calculated from non-relativistic models is obscure to say the least. However, the presence of extra branch cuts in the leading trajectories and their proximity to $\ell = -\frac{1}{2}$ may very well remain true. This would have important experimental implications.

It is well known[4] that the trajectory function can have no cut in E if $\ell > -\frac{1}{2}$. It was shown in Secs. III and IV that we can have branch points to the left of $\ell = -\frac{1}{2}$, with one of them close to $\ell = -\frac{1}{2}$ for an attractive potential with a strong repulsive core. This would imply that for the high ranking trajectories such as ρ, R, P and P' these cuts could be present, but only for rather large momentum transfer. However, if the particles involved have spin, these branch cuts are allowed to the right of $J = -\frac{1}{2}$. For example if a given Regge pole communicates with a spin $\frac{1}{2}$ - spin $\frac{1}{2}$ two particle channel (e.g., the ρ meson as a bound state of $N\bar{N}$), the trajectory can have a branch point up to $J = +\frac{1}{2}$ in the $\ell = J - 1$ spin state. In the case of ρ, this would be right in the region important for Regge-pole fitting.

This feature may be used to explain such puzzles as the polarization in the reaction $\pi^- p \to \pi^0 n$. In this case the only known high ranking trajectory is the ρ. If we assume that the ρ-trajectory function is real below threshold, there can be no polarization because the helicity flip and non-flip amplitudes are in phase. If we allow extra branch cuts in the ρ-trajectory, as mentioned above, the asymptotic behavior of the amplitude will necessarily be dominated by the two poles α_ρ^1 and α_ρ^2 corresponding to the colliding trajectories which give rise to the branch points. Between the two branch points, α_ρ^1 and α_ρ^2 are complex conjugates of each other, i.e., $\alpha_\rho^1 = \alpha_\rho^{2*} \equiv \alpha_\rho$.

If we write the spin $\frac{1}{2}$ - spin-0 differential cross section as:[19]

$$\frac{d\sigma}{dt} \propto \left\{ |f_{++}^t|^2 + |f_{+-}^t|^2 \right\} , \qquad \text{(VI.1)}$$

with f_{+-}^t and f_{++}^t the flip and non-flip amplitudes respectively, then the polarization is given by:

$$P \frac{d\sigma}{dt} \propto \mathrm{Im}(f_{++} f_{+-}^*) . \qquad \text{(VI.2)}$$

In the case of a ρ trajectory with extra branch points, we have, between the branch points

$$f^t_{++} = \beta_{++} \frac{(1 \pm e^{-i\pi\alpha})\, s^{\alpha}}{\sin\pi\alpha} + \beta^*_{++} \frac{(1 \pm e^{-i\pi\alpha^*})\, s^{\alpha^*}}{\sin\pi\alpha}, \qquad \text{(VI.3)}$$

where β_{++} is the appropriate residue functions. There will be a similar formula for f^t_{+-}. The cross section can then be written as:

$$\frac{d\sigma}{dt} \propto 4 \left\{ (\beta_{++}\beta^*_{++} + \beta_{+-}\beta^*_{+-}) \frac{\left[1 + \cosh(2\pi\alpha_I) \pm 2\cos(\pi\alpha_R)\cosh(\pi\alpha_I)\right]}{\cosh(2\pi\alpha_I) - \cos(2\pi\alpha_R)} \right.$$
$$\left. + \mathrm{Re}\left[\frac{(\beta_{++}\beta_{++} + \beta_{+-}\beta_{+-})}{(\sin\pi\alpha_\rho)^2} \exp\left[2i\alpha_I \ln s\right]\right]\right\} s^{2\alpha_R}, \qquad \text{(IV.4)}$$

where $\alpha_\rho = \alpha_R + i\alpha_I$. (Outside the cut region the cross section is given by the usual formula for two real Regge poles α_ρ^1 and α_ρ^2.) It is clear from Eq. (VI.4) that the differential cross section has an oscillatory component superimposed on the power behavior $s^{2\alpha_R}$, because of the imaginary part of α_ρ. However, this contribution would not be noticeable, even at extremely high energy, provided that α_I is not too large. The polarization can be written as:

$$P \frac{d\sigma}{dt} \propto -4\, r_{++}\, r_{+-} \sin(\theta_{++} - \theta_{+-}) \left\{ \frac{\sinh(2\pi\alpha_I) \pm 2\cos(\pi\alpha_R)\sinh(\pi\alpha_I)}{\cosh(2\pi\alpha_I) - \cos(2\pi\alpha_R)} \right\} s^{2\alpha_R},$$

(IV.5)

where $r_{++}\, e^{i\theta_{++}} = \beta_{++}$, $r_{+-} e^{i\theta_{+-}} = \beta_{+-}$.

Comparing Eq. (VI.5) and Eq. (VI.6), we notice that the polarization will have an s dependence given only by the oscillations in $\frac{d\sigma}{dt}$. As these are presumed to be not too significant, we conclude that in this scheme, the polarization will be essentially constant in energy.

A more striking phenomenon that might be explained by extra branch points in the trajectory function has been pointed out by Ringland and Thews[20] in the $\pi^- p \to \rho^0 n$ reaction. They have been able to obtain an upper bound for the spin density-matrix element $\mathrm{Re}\ \rho_{10}$ of the above reaction (effectively, the ρ polarization), by making the usual Regge pole dominance hypothesis. This bound is severely exceeded by the experimental data. One possible explanation is the existence of extra branch points in the trajectory and residue functions.

It is very likely that examples similar to the two mentioned above will be found as more processes involving spinning particles are investigated. There are, of course, alternative explanations to these apparent puzzles. Indeed both $\pi^- p \to \pi^0 n$ and $\pi^- p \to \rho^0 n$ polarization effects can also be explained by assuming an appropriate set of s-channel resonances, or the existence of Regge cuts, or by adding a low-lying trajectory to the amplitude.[21] However, each of these alternative hypothesis will predict a distinctive energy dependence which eventually may allow us to choose between them. The effect of the long range repulsion, as was shown in Section V, is to make the Regge trajectories of potential theory more like

the ones we expect to find in the relativistic problem. The trajectories now do not tend to turn over immediately above threshold, and they do not develop large imaginary parts close to $k^2 = 0$. To the extent that we can extend to relativistic problems intuition gained from potential situations, this behavior of the trajectories could be taken to indicate that the nuclear force has a large long range repulsive component.[22]

ACKNOWLEDGMENTS

We would like to thank Professor G. F. Chew for stimulating discussions. One of us (N.F.B.) would also like to thank Professor G. F. Chew for his hospitality in the Theoretical Group of the Lawrence Radiation Laboratory.

FOOTNOTES AND REFERENCES

* This work was performed under the auspices of the U. S. Atomic Energy Commission.

† Fellow of the Consejo Nacional de Investigaciones Cientificas y Técnicas, Argentina while a major part of this work was being carried out.

1. A. Amadzadeh, P. G. Burk, and C. Tate, Phy. Rev. 131, 1315 (1963).

2. Y. I. Azimov, A. A. Ansel'm, and V. M. Shekhter, Soviet physics JETP 17, 246 (1963); 17, 726 (1963).

3. C. Lovelace and D. Masson, Nuovo Cimento 26, 472 (1962).

4. R. G. Newton, The Complex J-Plane (W. A. Benjamin, Inc., N. Y. 1964).

5. M. Moravcsik, The Two-Nucleon Interaction (Clarendon Press, Oxford, 1963).

6. See p. 31, Eqs. (5-12) of Ref. 4.

7. We assume $V(r)$ decreases rapidly as $r \to \infty$, so that no divergence will occur at the upper limit.

8. See lemma on p. 22 of Ref. 4.

9. Y. I. Azimov, et al, in Ref. 2, have made is plausible that all trajectory functions are different branches of the same analytic function.

10. See Ref. 2 for details of the following.

11. Q_ℓ is the usual Legendre function of the second kind and

the properties of R_ℓ can be found from Eq. (1) in p. 390 of G. N. Watson, Theory of Bessel Functions (The Macmillan Company, 1944).

12. P. Kaus, Nuovo Cimento 29, 598 (1963).

13. A. E. A. Warburton, Nuovo Cimento 32, 122 (1964); 37, 267 (1965).

14. When two poles approach each other for real k^2, their identity after collision is determined by giving k^2 a small positive imaginary part.

15. If the coupling is strong several such leading trajectories may appear. See Ref. 2.

16. The zeros of the first factor in Eq. (IV.9) will cancel in the S matrix with the corresponding zero in $f_+(\ell,k)$.

17. R. Haymaker, Bulletin of the American Physical Society 12, 561 (1967).

18. As it is well known, a trajectory approaches its threshold value like $k^{2\ell_0+1}$. If $\ell_0 < 0$, the trajectory moves into the complex ℓ plane at an angle greater than $\frac{\pi}{2}$.

19. M. Jacob and G. F. Chew, The Strong Interaction Physics (W. A. Benjamin, Inc., N. Y., 1964).

20. G. Ringland and R. Thews, A Bound for the Effective Polarized in ρ Production in A Regge Pole Exchange Model, Lawrence Radiation Laboratory Report UCRL-17474, 1967. (unpublished)

21. For example, see C. Chiu and J. Finkelstein, Suggestive Features in πN Charge-Exchange Polarization Associated with Regge Cuts, Lawrence Radiation Laboratory Report UCRL-17318, 1967. (to be published in Nuovo Cimento Letters)

22. G. F. Chew, Phys. Rev. Letters 16, 60 (1966).

Table I: Slope and imaginary part of two trajectories that have an $\ell = 1$ resonance at $k^2 = 2.04$, computed at the resonance point. Case 1, $g_1 = 20.0$, $\mu_1 = 0.5$, $g_2 = -35.0$, $\mu_2 = 1$. Case 2, $g_1 = 16.41$, $\mu_2 = 0.5$, $g_2 = -30$, $\mu_2 = 1$.

	Slope	Im α	Γ
Case 1	0.13	0.043	0.66
Case 2	0.13	0.087	1.34

FIGURE CAPTIONS

Fig. 1. Trajectory switch over from short range repulsion to long range attraction, $(g_1 < 0,\ g_2 > 0)$, showing the complex ℓ-plane and the analytic structure of the complex k^2-plane for the branch of $\alpha(k^2)$ that goes to -2 as $|k^2| \to \infty$. The numbers at the branch points indicate the collision partners.

(a) $g_1 = 0$

(b) $|g_1| < |g_2|$, $\left|\frac{g_1}{\mu_1}\right| > \left|\frac{g_2}{\mu_2}\right|$

(c) $|g_1| = |g_2|$,

(d) - (h) decreasing g_2

(i) $g_2 = 0$

Fig. 2. Spiraling of complex threshold trajectories as $k^2 \to 0^-$. This configuration corresponds to Figure 1d.

Fig. 3. Trajectory switch over from short range attraction to long range repulsion $(g_1 > 0,\ g_2 < 0)$, showing the complex ℓ-plane and the analytic structure of the complex k^2-plane for the branch of $\alpha(k^2)$ that goes to -2 as $|k^2| \to \infty$.

(a) $g_1 = 0$

(b) $\left|\frac{g_1}{\mu_1}\right| = \left|\frac{g_2}{\mu_2}\right|$

(c) $|g_1| = |g_2|$

(d) - (h) decreasing g_2

(i) $g_2 = 0$

Fig. 4. Complex ℓ-plane for trajectories from -2 and -1, for potential $g_1 = -4.0$, $\mu_1 = 0.5$; $g_2 = 4.5$, $\mu_2 = 1$.

Fig. 5. Real part of $\alpha(k^2)$ versus k^2 for trajectories in Fig. 4. Dotted line indicates region where trajectories are complex conjugates.

Fig. 6. Imaginary part of $\alpha(k^2)$ versus k^2 for trajectories in Fig. 4. Dotted line is the trajectory from -2, solid line is trajectory from -1.

Fig. 7. Complex ℓ-plane for trajectories from -1, -2, -3, for the potential $g_1 = -4.$, $\mu_1 = 0.25$, $g_2 = 4.5$, $\mu_2 = 1$.

Fig. 8. Complex ℓ-plane for trajectories from -1, -2, for the potential $g_1 = 15.0$, $\mu_1 = 0.5$, $g_2 = -20.0$, $\mu_2 = 1.0$ showing an S-wave resonance.

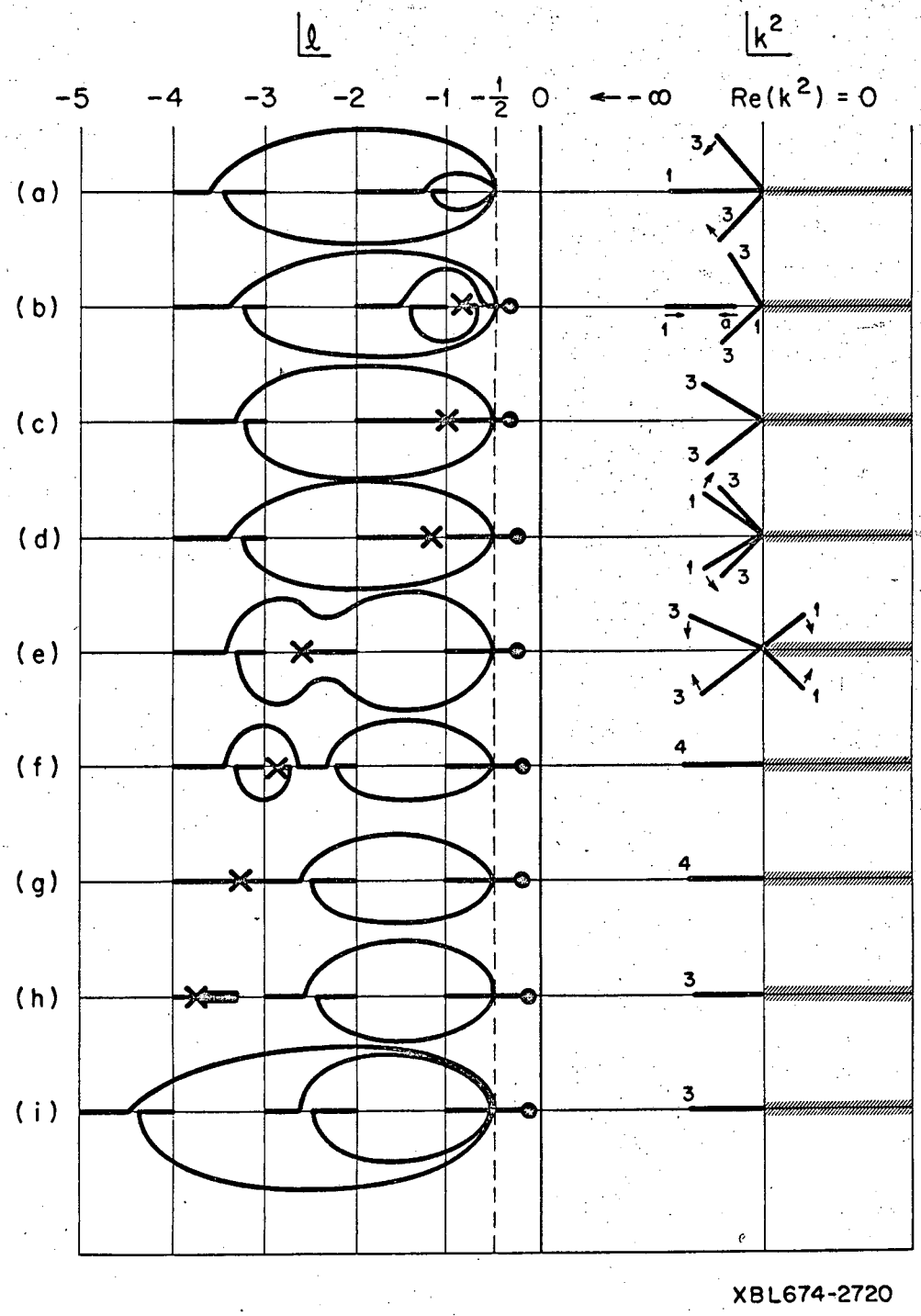

Fig. 1

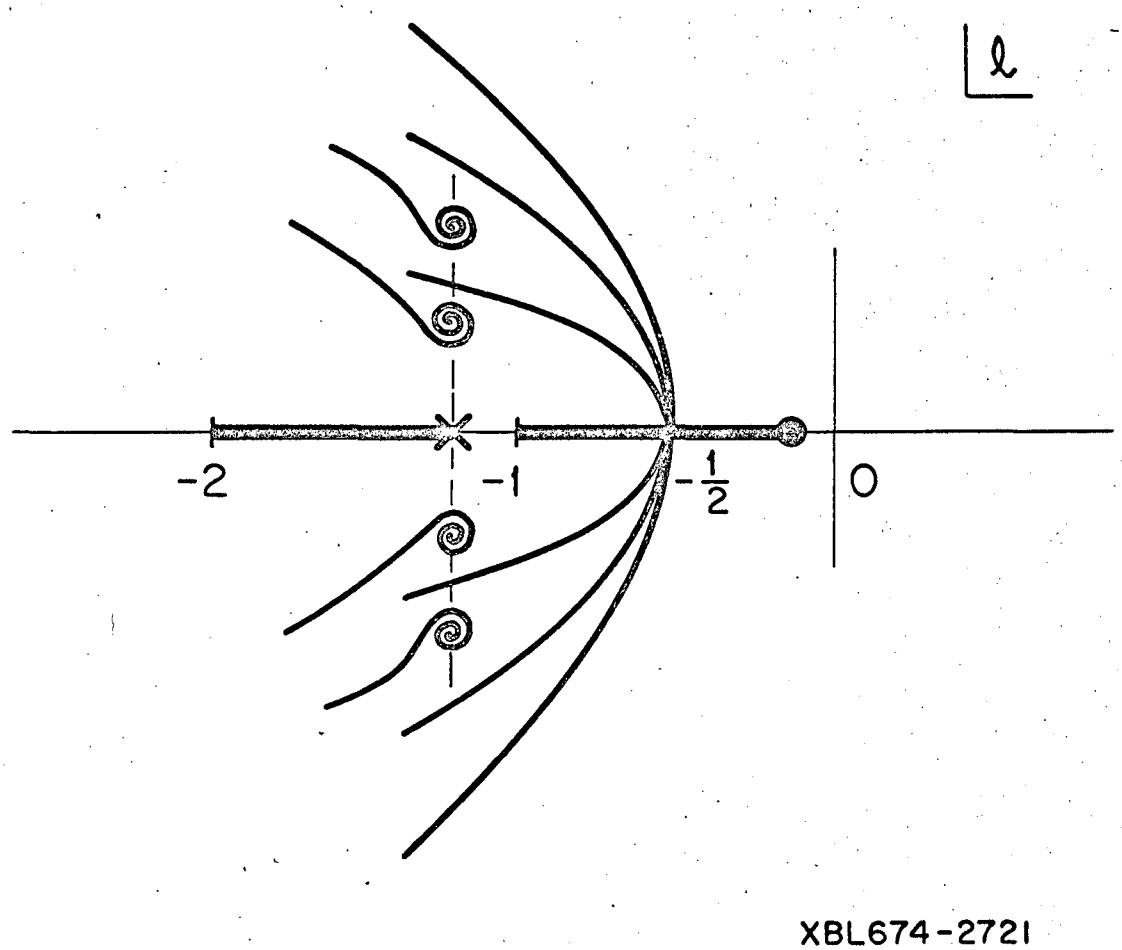

Fig. 2

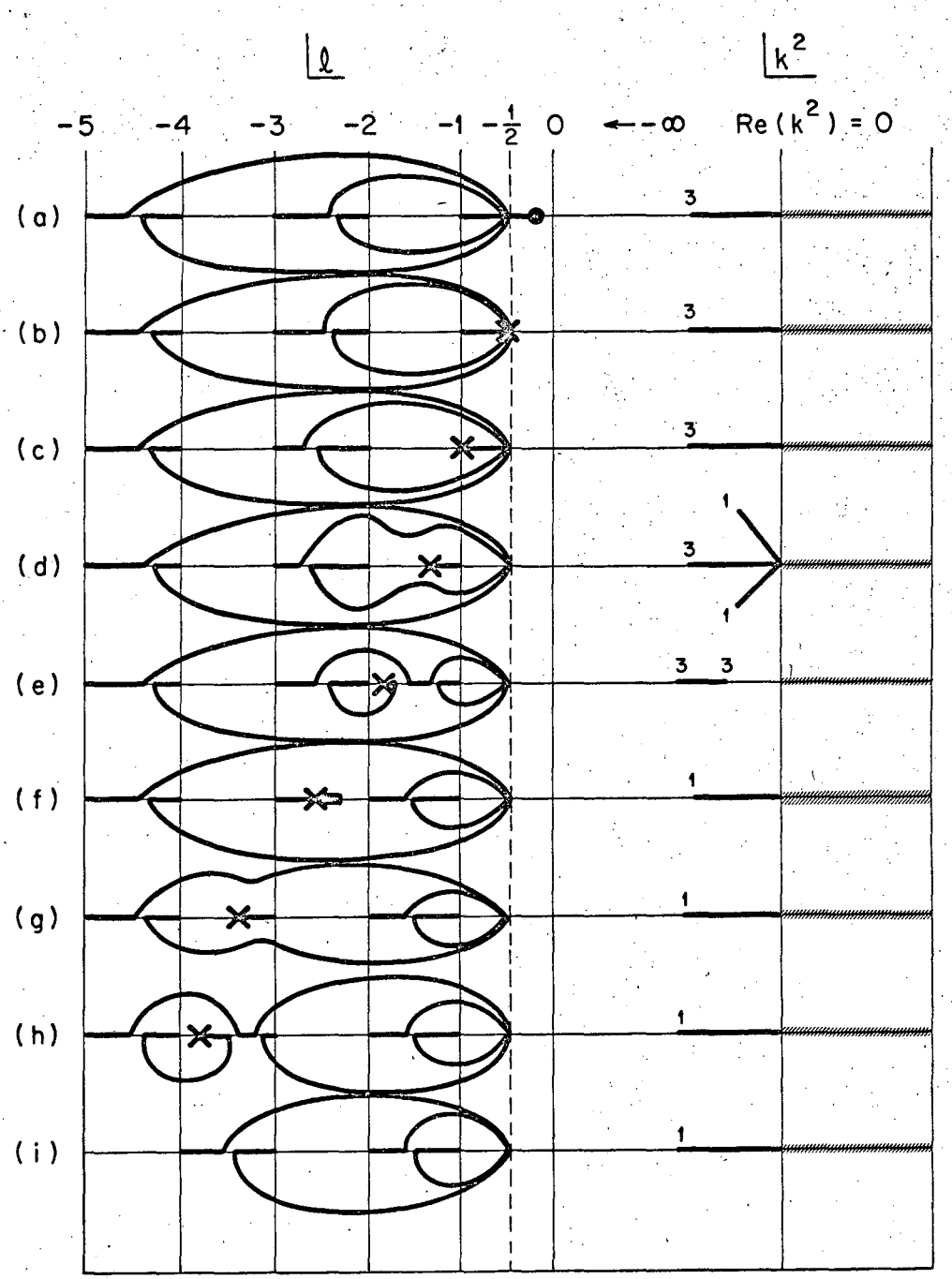

XBL674-2722

Fig. 3

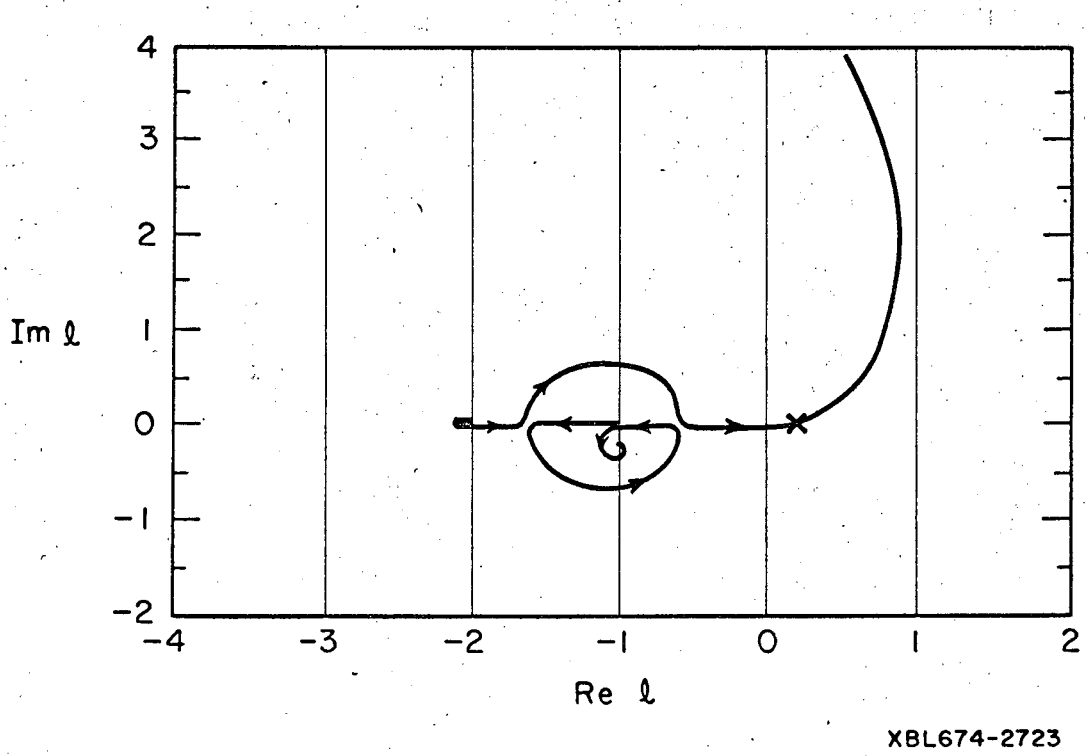

Fig. 4

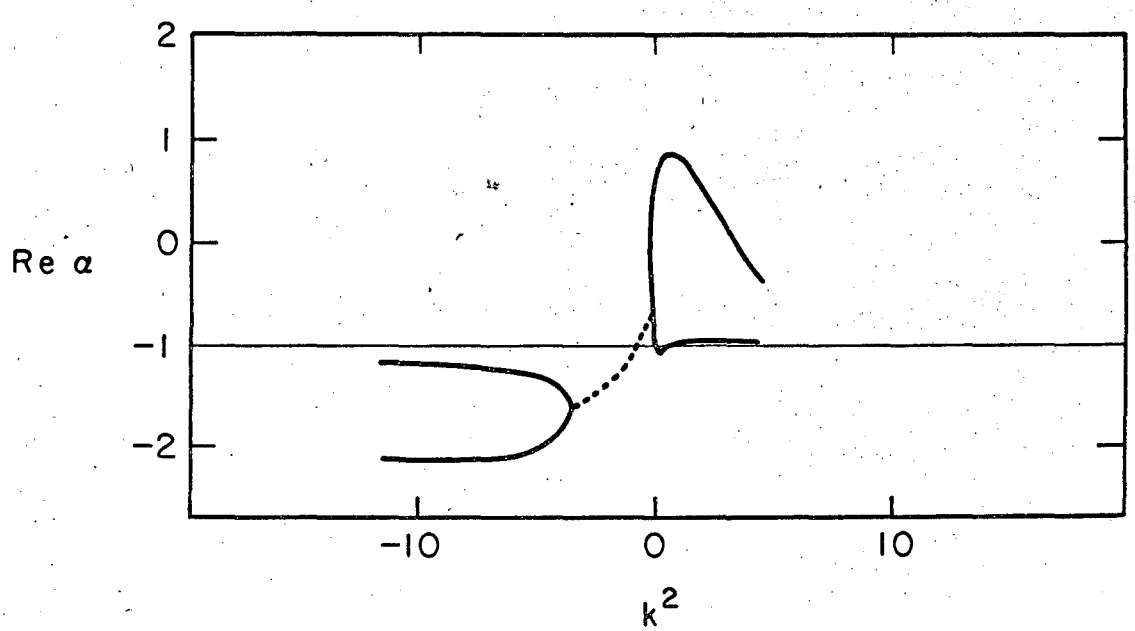

XBL674-2724

Fig. 5

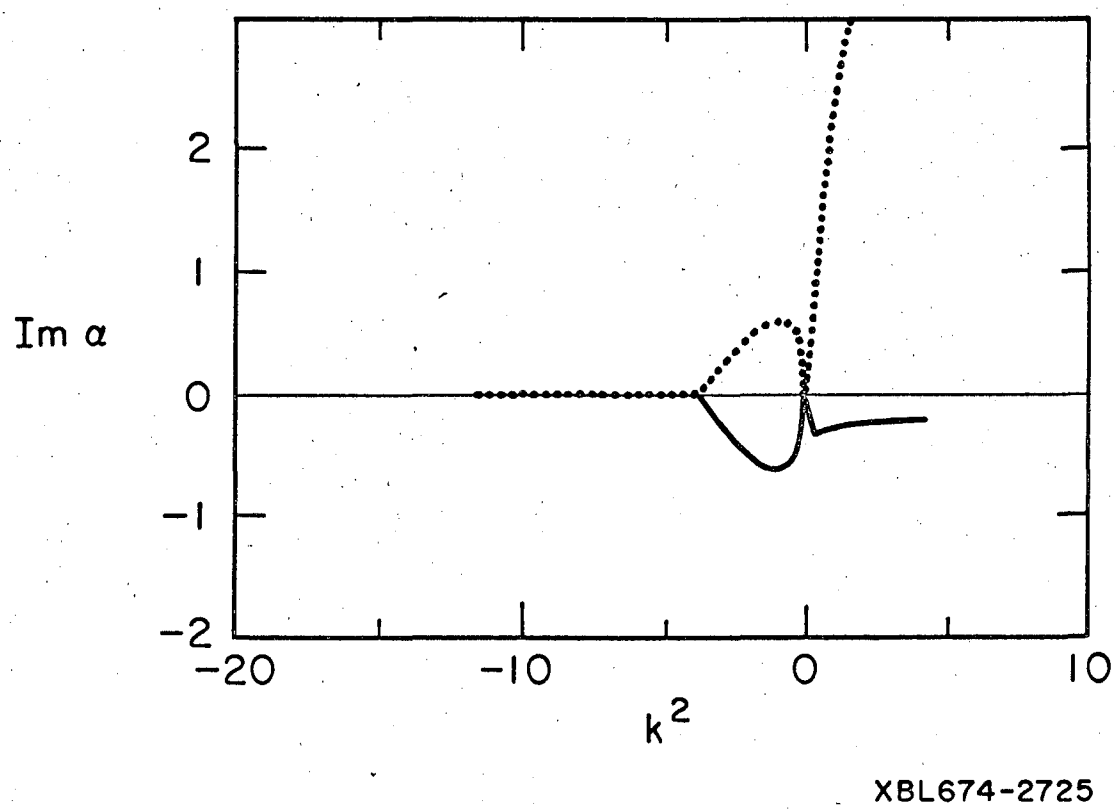

Fig. 6

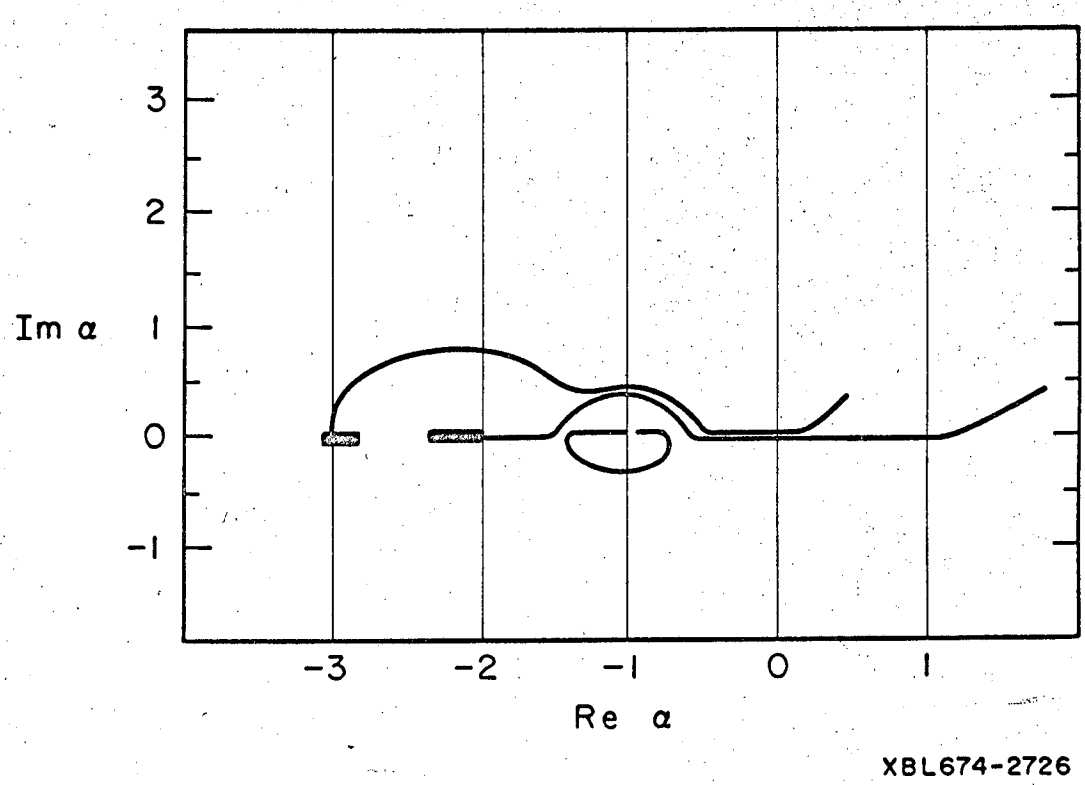

Fig. 7

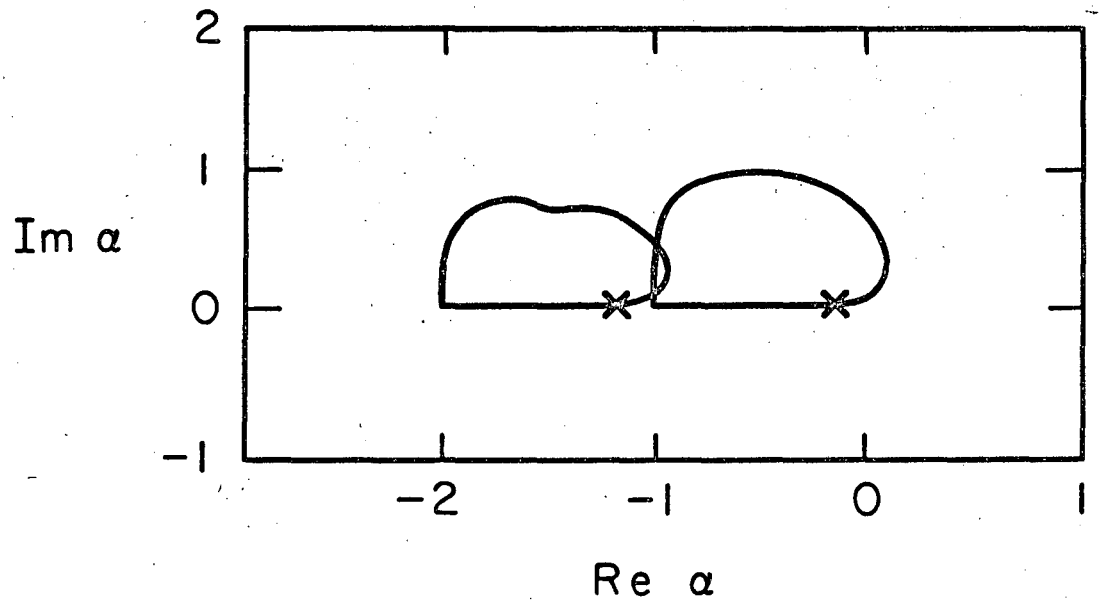

XBL674-2727

Fig. 8

This report was prepared as an account of Government sponsored work. Neither the United States, nor the Commission, nor any person acting on behalf of the Commission:

A. Makes any warranty or representation, expressed or implied, with respect to the accuracy, completeness, or usefulness of the information contained in this report, or that the use of any information, apparatus, method, or process disclosed in this report may not infringe privately owned rights; or

B. Assumes any liabilities with respect to the use of, or for damages resulting from the use of any information, apparatus, method, or process disclosed in this report.

As used in the above, "person acting on behalf of the Commission" includes any employee or contractor of the Commission, or employee of such contractor, to the extent that such employee or contractor of the Commission, or employee of such contractor prepares, disseminates, or provides access to, any information pursuant to his employment or contract with the Commission, or his employment with such contractor.